The Effect of pH on Electroless Ni-Fe-P Alloy Plating on Poplar Veneer

Tongcheng Guo, Yu Wang, and Jintian Huang*

Ni-Fe-P alloy coating was fabricated on poplar veneer substrates by an electroless plating method. The influence of pH on coating structure, elementary composition, thickness, crystal structure, surface resistivity, and magnetism were evaluated. The results indicated that when the plating solution pH was 9.5, the Ni-Fe-P coating had a crystal structure. The coating consisted of lamellar metal particles, and the thickness increased to 111 μm. This plated veneer showed soft magnetic properties. In contrast, when the plating solution pH was 4.5, the Ni-Fe-P coating had mainly an amorphous structure. The coating consisted of spherical metal particles, and the thickness was 67 μm. After 600 °C heat treatment, this plated veneer shifted to a crystalline structure and exhibited soft magnetic properties. In two kinds of plated veneers, the lateral direction resistivity was two times greater than the longitudinal direction resistivity.

Keywords: Plating N-iFe-P alloy; pH; Soft magnetic properties; Heat treatment

*Contact information: College of Material Science and Art Design, Inner Mongolia Agricultural University, Hohhot 010018, China; *Corresponding author:jintian_h@163.com*

INTRODUCTION

A NiFe alloy is a permalloy, where the nickel content ranges from 30% to 90% (Mamin *et al*. 1989; Zhou *et al*. 2009). NiFe alloys exhibit excellent electrical conductivity and magnetic performance. High magnetic permeability and low coercive force make NiFe alloys suitable for magnetic shielding materials, alloy cores, and transformer preparation (Duhamel *et al*. 2005; Zhou *et al*. 2005; Liu *et al*. 2010). In addition, their processability and corrosion resistance are also excellent because of the relatively high Ni content. NiFe alloys can be prepared by hydrothermal method (Liao *et al*. 2006), metal-organic decomposition method (Lai *et al.* 2009), electrochemical deposition method (Cheung *et al*. 1995), and solution reduction (Wei *et al*. 2006; Moustafa and Daoush 2007; Vitta *et al*. 2008; Wang *et al*. 2008; Qin *et al*. 2009). The electroless plating method is a solution reduction method, and it is the ideal option to prepare wood-NiFe alloy composites.

There has been research on the electroless plating of metal on wood surfaces (Nagasawa *et al*.1999). This wood-metal composite combines light quality and excellent electrical conductivity, as well as magnetism from two components. Current research focuses on plating copper and nickel on wood (Wang *et al*. 2011, 2013; Guo *et al*. 2016; Pan *et al*. 2016). In past research, the Ni-Fe-P alloy was deposited on a wood surface in alkaline conditions (Shi *et al*. 2015; Wang *et al*. 2015).

In this article, the electroless plating principle can be expressed by the following reaction formula:

$$Ni^{2+}(Fe^{2+})+H_2PO_2^-+H_2O \rightarrow Ni^0(Fe^0)+H_2PO_3^-+2H^+ \quad (1)$$

The specific reaction process is divided into the following steps:

$$H_2PO_2^- + H_20 \rightarrow H^+ + H_2PO_3^- + 2\,H_{Adsorption} \quad (2)$$

$$Ni^{2+}(Fe^{2+}) + 2\,H_{Adsorption} \rightarrow Ni^0(Fe^0) + 2\,H^+ \quad (3)$$

$$H_2PO_2^- + H_{Adsorption} \rightarrow H_2O + OH^- + P \quad (4)$$

$$H_2PO_2^- + H_2O \rightarrow H_2PO_3^- + H_2\uparrow \quad (5)$$

$$H_2PO_2^- + H_2O \rightarrow H_2PO_3^- + H_2\uparrow \quad (6)$$

$$2\,H \rightarrow H^2\uparrow \quad (7)$$

At last Fe, Ni, and P co-deposited to form an alloy coating:

$$xFe+yNi+zP \rightarrow Ni_y\,Fe_x\,P_z \quad (8)$$

Following the pH increase, the deposition rate of Ni (Fe) increased, while the deposition rate of P will have declined, so the P content of the coating decreased. Conversely, when reducing the pH value of the plating solution, the deposition rate of P increased, while the deposition rate of Ni (Fe) will have declined. However, the deposition rate of Fe is slow in acidic solution. Accordingly, the coating composition was changed, depending on the pH value. The properties such as coating structure, crystal structure, thickness, surface resistivity, and magnetism of alloy coatings, which were prepared under different pH conditions, were investigated. The coating performance after heat treatment was also evaluated.

EXPERIMENTAL

Materials

Poplar veneer was obtained from the Sen Ming wood product factory, Hebei Province, China, with a thickness of 1 mm and format for φ4 mm. The composition of the electroless plating solution and specific conditions are listed in Table 1.

Table 1. Conditions for Electroless Deposition

Component	Contents	Conditions
$(NH_4)_2Fe(SO_4)_2•6H_2O$ (Ammonium iron(II) sulfate)	30 g/L	Temperature 85°C pH=4.5 pH=9.5
$NiSO_4•6H_2O$ (Nickelous sulfate)	30 g/L	
$NaH_2PO_2•H_2O$ (Sodium hypophosphite)	60 g/L	
$Na_3C_6H_5O_7•2H_2O$ (Sodium citrate)	30g/L	

Preparation of Wood Metallization

Activation treatment

The veneer substrate was soaked in a $(NH_4)_2Fe(SO_4)_2·6H_2O$ and $NiSO_4·6H_2O$ solution containing 12 g/L of hydrochloric acid (HCl) for 9 min at room temperature. It was then transferred to a $NaBH_4$ solution containing 12 g/L of sodium hydroxide (NaOH) for about 90s.

Electroless plating method

The plating solution was prepared according to the formulation in Table 1. The veneer substrate (in solution form) was constantly stirred for 40 min. After the reactions had run to completion, the plated veneer was dried for 30 min in a vacuum oven (DH-101-2-S-type, Yi Heng Scientific Instruments, Shanghai, China) to measure the properties. The preparation of the composite is presented schematically in Fig. 1.

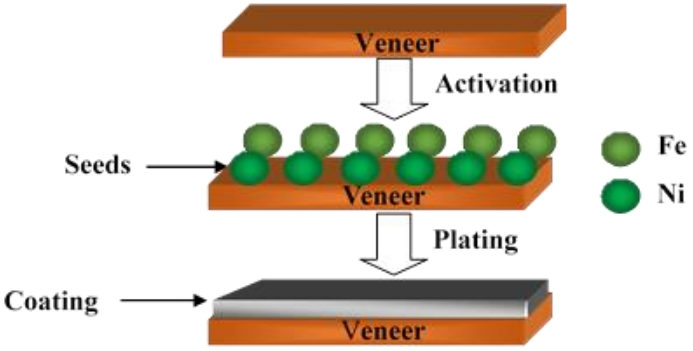

Fig. 1. Schematic of the electroless plating process of NiFe alloy on veneer

Characterization

Scanning electron microscopy (SEM)

The coating surface morphology and cross section were obtained using a Quanta scanning electron microscope (FEG-QUANTA650, FEI Co., Hillsboro, OR, USA).

X-ray diffraction (XRD)

X-ray diffraction was conducted on an XRD-6000 diffractometer (Shimadzu, Tokyo, Japan) to characterize the crystal structure of the plated veneer and determine the grain size (Cu target, λ = 0.154056 nm, scanning range 20° to 80°, and scanning speed of 2°/min). Jade 5.0 software (Materials Data Inc., Livermore, CA, USA) was used to analyze XRD patterns in the diffraction angle ranged from 20° to 80°.

Electrical property

The resistance and conductivity of the plated wood surface was tested *via* a FT-201 four-point probe resistance meter (Four Probes Technology Company, Guangzhou, China) in the longitudinal and lateral coating directions.

Magnetic characterization

The magnetic hysteresis loops of the plated veneer were determined with a PMS-XL-7 VSM meter (Lake Shore Company, CA, USA).

Differential scanning calorimeter

The crystallization temperatures of coating were measured at a heating rate of 10 °C/min by a TA Q600 thermo gravimetric analysis instrument (TA Instruments, Newcastle, DE, USA) in an atmosphere of pure nitrogen gas.

Heat treatment

The FSX2-12-15N chamber electric furnace (HBYQ Company, Tianjin, China) was used to heat the plated veneer at 600 °C.

RESULTS AND DISCUSSION

Morphology

Figure 2 shows the effects of different solution pH on the veneer surface morphology. Figures 2a and 2b display two plated veneers surfaces covered by a metallic film; the inset images show that the coating structure is related to solution pH. At pH 9.5, the coating consisted solely of lamellar metal particles, and the coating structure was compact and uniform, with fewer defects (Fig. 2a). In contrast, at pH 4.5, the entire coating was distributed by independent micron spherical metal particles, and the coating was less continuous than before. The cause of this phenomenon is that NiFe alloy deposition is a typical anomalous co-deposition process. The reactivity of Fe^{2+} and Ni^{2+} are significantly different, such that the reduction rate of Fe^{2+} was very low in acidic solution and the coating can be regarded as pure Ni. However, in alkaline solution, the reduction rate of Fe^{2+} apparently increased, and the NiFe alloy coating deposited on poplar veneer substrate surface.

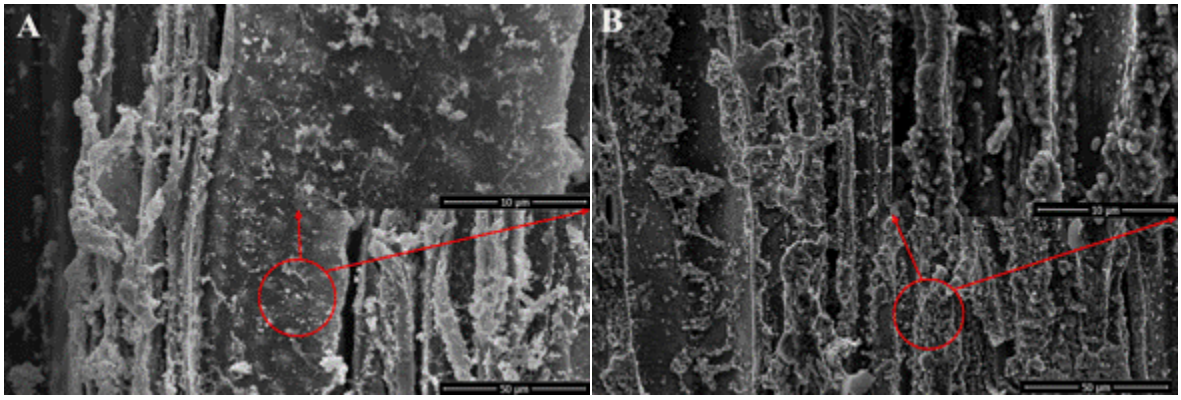

Fig. 2. Surface morphology of metallized poplar veneer at different (A) pH 9.5 and (B) pH 4.5. The inset images show 10000× amplification.

EDS Analysis

The energy dispersive spectrums of different solution pH plated veneers are depicted in Fig. 3, and the coating element composition is listed in Table 2. Table 2 indicates that all coatings contained Ni-Fe-P. However, each element proportion was different. In acidic conditions, the Fe content was 1.08% in the coating, and the P content was high, indicating a typical high phosphorus Ni-P coating. However, in alkaline conditions, the Fe content increased from 1.08% to 12.56% (an 11-fold increase). The Ni-Fe-P alloy coating was a typical low phosphorus coating because the P content decreased to 3.83%. Figure 3a indicates that the O content was elevated, suggesting that the alloy coating was easily oxidized. EDS analysis demonstrated that the alloy coating element composition changed following the reactant concentration difference and the solution pH variation. This changing of the composition leads to marked differences in the coating surface morphology.

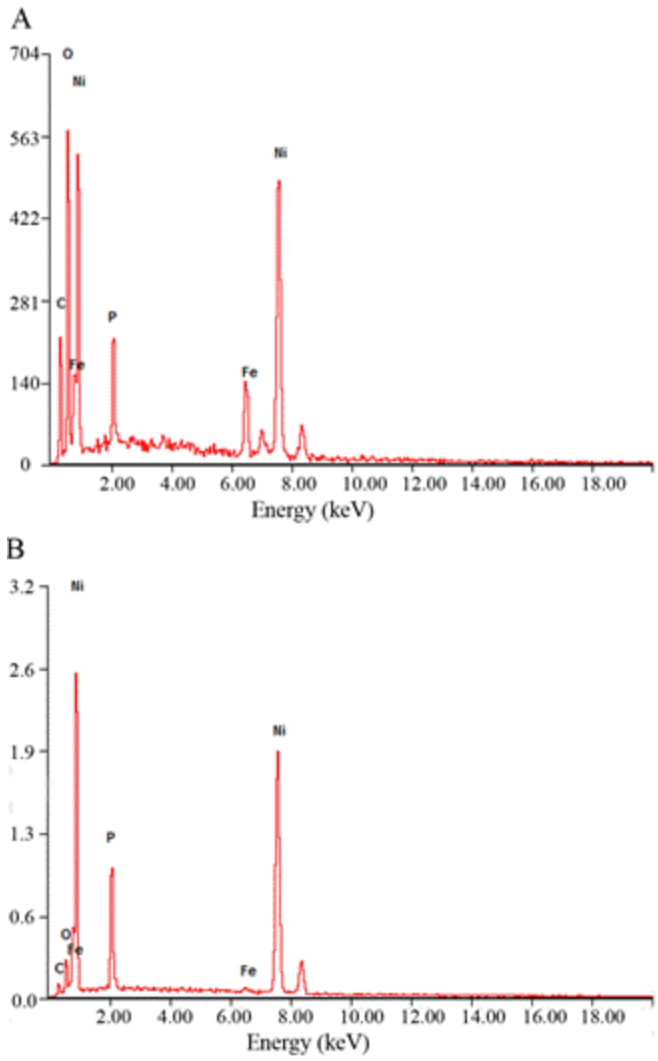

Fig. 3. EDS spectra of metallized poplar veneer (A) pH 9.5; (B) pH 4.5

Table 2. Coating Composition at Different pH

pH	Ni (%)	Fe (%)	P (%)	C (%)	O (%)
9.5	70.15	12.56	3.93	3.55	9.81
4.5	81.42	1.08	9.38	3.83	4.29

Cross-Sectional Morphology

The coating thickness of a veneer cross-section is presented in Fig. 4. The coating thickness increased gradually from 67 μm to 110.6 μm, which was nearly twice the original thickness, as a consequence of the change in conditions from acidic to alkaline. In acidic conditions, the Ni^{2+} deposition rate increased remarkably. The Ni particles were not deposited on the veneer substrate surface, but instead suspended in the solution. This is the reason why the coating thickness in Fig. 4a was just 67 μm. Under alkaline conditions the deposition rates of Ni^{2+} and Fe^{2+} were appropriate, so the coating thickness increased quickly (Fig.4b). Figure 4 also illustrates that these two coatings were tightly stacked by metal particles that have fewer defects.

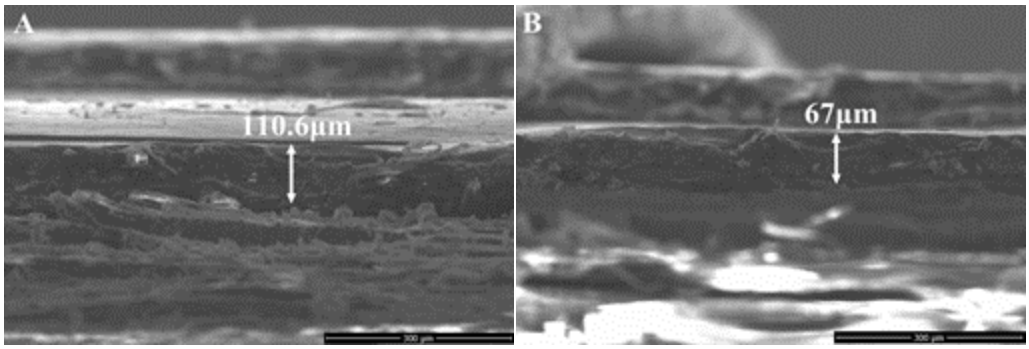

Fig. 4. Cross-sectional morphology (A) pH 9.5; (B) pH 4.5. The thickness was 110.6 μm and 67 μm, respectively.

X-Ray Diffraction Analysis

The X-ray diffraction patterns are shown in Fig. 5. There was only one diffraction peak at 2θ = 22° in sample B, which is the characteristic diffraction peak of cellulose. Besides this peak, there are three diffraction peaks at 2θ = 45.64°, 52.92°, and 77.92° in sample B (shown in Fig.2), but those diffraction peaks are not standard crystal diffraction peaks, just sharp diffraction peaks that appear in the predominantly amorphous diffuse scattering peaks. According to EDS analysis, in acidic solution, the P content was high, and the deposition rate was very fast, making the coating exhibit amorphous properties. However, the sample A XRD pattern reflected a crystalline structure, and the diffraction peaks of NiFe alloy (111), (200), and (220) were apparent. These diffraction peaks indicated the presence of NiFe alloy on the poplar veneer substrate surface. A comparison of sample A and B showed that the coating crystalline structure of the plated veneer shifted from amorphous to crystalline. The cellulose diffraction peaks disappeared, indicating that the sample A coverage fraction was higher than sample B.

The diffraction peaks of sample B at 2θ = 47.84°, 55.78°, and 77.48° were compared with the reference PDF card 37-0474 (permalloy standard pattern), and face-centered cubic permalloy diffraction peaks were identified. According to crystallography (Mohammadi *et al*. 2016), in the deposition of permalloy, Ni^{2+} and Fe^{2+} are easily deposited on the (200) crystal face because the bulk density of the atomic planes is lower in this crystal face. However, in the current study, the solution pH was 9.5, causing Ni^{2+} and Fe^{2+} to become colloidal hydroxides such as $Fe(OH)^{+}$ and $Fe(OH)_2$. The energy of the (200) crystal face improved because of the preferential deposition of colloidal hydroxides on the (200) crystal face. Thus, the preferred orientation of crystal growth transformed (200) to (111). Using the Sherrer formula (Eq. 9), the half-peak width measured from NiFe alloy (111) crystal plane was used to calculate the grain size; the average crystallite size was approximately 8.6 nm (shown in Table 3). According to the above analysis, there were no grains and grain boundaries because the sample B coating was mainly amorphous. So one cannot be calculated the average grain thickness by Sherrer formula.

$$D = \frac{k\lambda}{\beta \cos\theta} \quad \text{(Sherrer formula)} \qquad (9)$$

In Eq. 9, k is the Scherrer constant (1), D is the average grain thickness (nm) in the perpendicular direction of the crystal plane, β is the half-width of the diffraction peak, and λ is the X-ray wavelength.

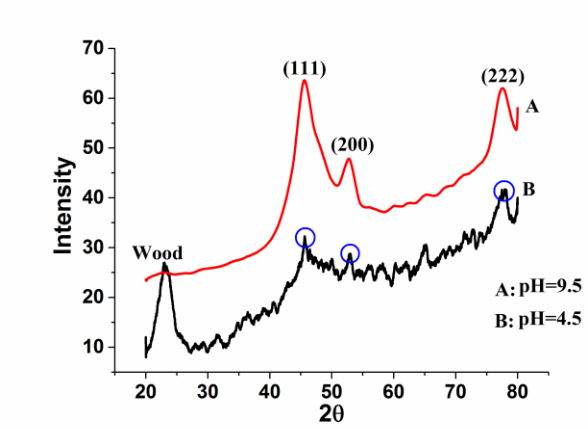

Fig. 5. X-ray diffraction analysis

Table 3. Integral Breadth and Calculated Crystallite Size

pH	Integral Breadth (β; radians)	Crystallite Size (nm)
9.5	1.085	8.6

Surface Resistivity

Figure 6 demonstrates that as the solution pH increased, the plated veneer surface resistivity in the longitudinal and lateral directions tended to decrease, and the conductivity increased. According to morphology and XRD analyses, in the alkaline condition, the coating is crystalline structure, and the metal particles accumulate uniform and compact. Furthermore, the surface resistivity of plated poplar veneer exhibited profound differences in the longitudinal and lateral directions. The resistivity of the lateral direction was twice that of the longitudinal direction; the surface resistivity showed anisotropy.

Poplar veneer substrate is a typical anisotropic material. The longitudinal direction wood cell density is much higher than lateral direction; more defects appear in the lateral direction, affecting the conductivity. However, the probe hardness was higher, when the plated veneer was squeezed by test probes, allowing the formation of craters in the lateral direction. Therefore, the resistivity in the lateral direction was higher than in the longitudinal direction.

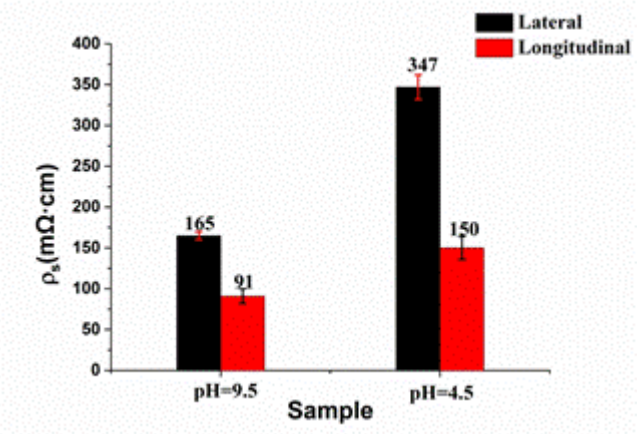

Fig. 6. Resistivity of electroless plated veneer in the lateral and longitudinal directions

Magnetic Characterization

The hysteresis loops at room temperature are shown in Fig. 7. Magnetization occurs when the intensity of an external magnetic field less than 1000 G and the coercivity (H_c) is 160 G. At pH 9.5, the plated veneer exhibited a soft magnetic property, which is similar to previous results (Xue *et al*. 2016). In contrast, the hysteresis loop of the electroless plated veneer at pH=4.5 was ferromagnetic, the saturation magnetizations (MS) was 3.3 emu/g, the coercivity (H_c) was 1627 G, and the remanence (M_r) was 3.05 emu/g.

Traditional magnetization theory regards that soft magnetic property can influence grain size; a smaller grain size results in a lower soft magnetic property. However, Herzer (1989) believes that nano grain morphology improves the soft magnetic properties. In this study, the average crystallite size was about 8.6 nm (according to XRD analysis). Thus, all samples exhibited excellent soft magnetic properties.

Table 4 shows that the saturation magnetizations (M_S) was transformed from 4.80 emu/g to 10.5 emu/g. There are two reasons for this trend. First, the saturation magnetization of Fe (217.5emu/g) was higher than that of Ni (54.4emu/g), so the higher Fe content plated veneer had a higher saturation magnetizations. Secondly, the increased P content decreased the saturation magnetization.

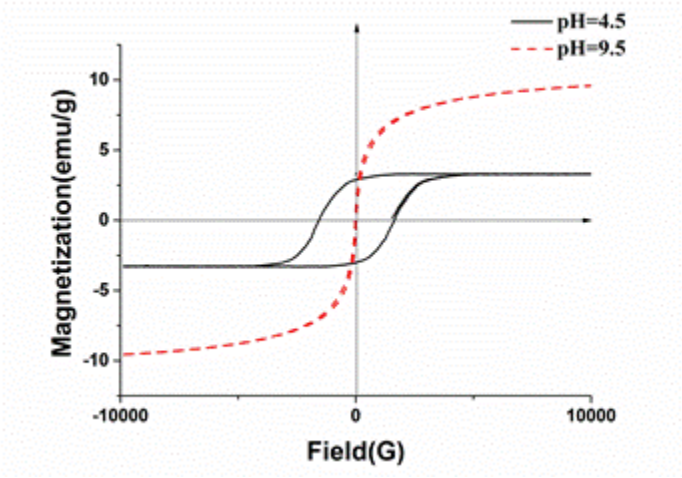

Fig. 7. Hysteresis loops of the electroless plated veneer

Table 4. Magnetic Properties of the Electroless Plated Veneer

pH	Saturation Magnetization (Ms) (emu/g)	Coercivity (Hc) (G)	Remanence (Mr) (emu/g)
9.5	10.5	160	0.6
4.5	3.3	1627	3.05

DSC Analysis

The phase transformation behavior of electroless NiFe deposition was studied using differential scanning calorimetry (DSC) (Fig. 8). The two DSC curves exhibited a distinct exothermic peak from 296 to 322 °C. This exothermic peak is attributed to pyrolysis of cellulose. There was another endothermic peak at 552 °C, which was attributed to the Ni-P structural transition from amorphous to crystalline. DSC analysis also established that the amorphous structure can be obtained from acidic solution.

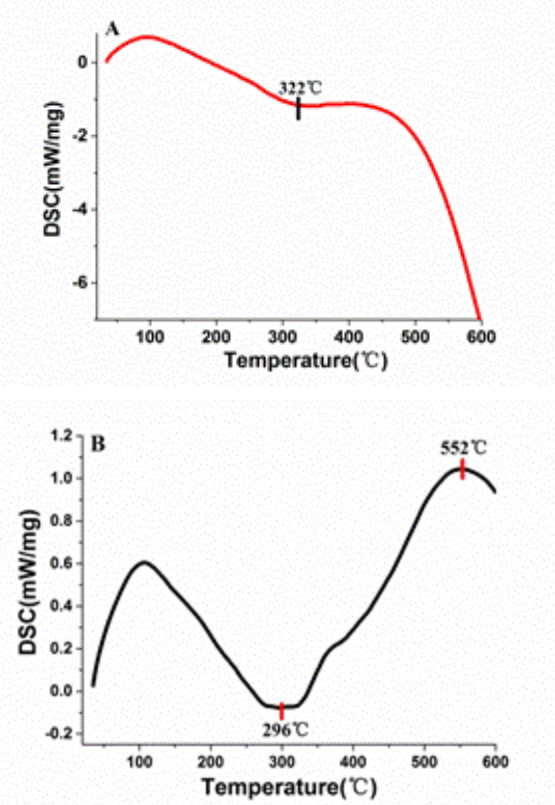

Fig. 8. DSC curve of the electroless veneer (A) pH 9.5; (B) pH 4.5.

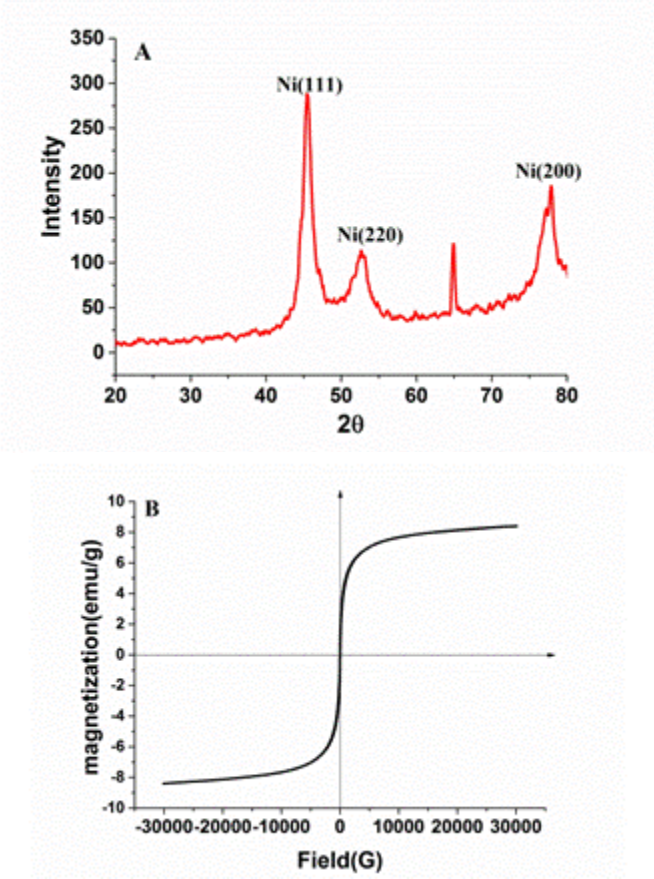

Fig. 9. X-ray diffraction analysis (A) and hysteresis loops (B) of heat treatment plated veneer

Characterization after Heat Treatment

The amorphous plated veneer was heated to 600 °C for 30 min in a chamber electric furnace. The XRD pattern and hysteresis loop of the coating after heat treatment are shown in Fig. 9. Figure 9a demonstrates that the coating structure was crystalline after heat treatment. The hysteresis loop reflects that the coating exhibited a soft magnetic property, and the remanence (M_r) decreased obviously. The saturation magnetization was 8.4 emu/g. Thus, after 600 °C heat treatment process, the acidic condition coating shifted from an amorphous structure to the crystalline structure.

CONCLUSIONS

1. When the solution pH was shifted from 4.5 to 9.5, the coating structure changed from lamellar to spherical, and the thickness increased from 67 μm to 111 μm.
2. In acidic conditions, the Ni-Fe-P was mainly an amorphous coating. In alkaline conditions, the Ni-Fe-P was a typical crystalline alloy coating, and the average grain size was 8.6 nm.
3. The surface resistivity had obvious anisotropy, and the lateral direction measurement was approximately twice the measurement in the longitudinal direction.
4. The plated veneer exhibited a soft magnetic property in the alkaline condition, and the saturation magnetizationwas10.5 emu/g.
5. After heat treatment, the coating (obtained from acidic condition) appeared crystalline with a soft magnetic property. The saturation magnetization was 8.4 emu/g.

ACKNOWLEDGMENTS

This work was supported by the Inner Mongolia Agricultural University Commercialization Plan Projects (Grant No. CGZH2013006), and the Science Research Innovation Projects of the Inner Mongolia Autonomous Region for Graduate (Grant No. B20151012911).

REFERENCES CITED

Cheung, C., Djuanda, F., Erb, U., and Palumbo, G. (1995). "Electrodeposition of nanocrystalline Ni-Fe alloys," *Nanostruct. Mater* 5(5), 513-523. DOI: 10.1016/0965-9773(95)00264-F

Duhamel, C., Champion, Y., Tencé, M., and Walls, M. (2005). "Synthesis of controlled-chemistry ultrafine Fe_xNi_{1-x}ferromagnetic powders," *J. Alloy Compd.* 393(1), 204-210. DOI:10.1016/j.jallcom.2004.10.041

Guo, T.C., Wang, Y., and Huang, J. T. (2016). "Studies of electroless copper plating on poplar veneer," *BioResources* 11(3), 6920-6931. DOI: 10.15376/biores.11.3. 6920-6931

Herzer, G. (1989). "Grain structure and magnetism of nanocrystalline ferromagnets," *IEEE Transactions on Magnetics* 25(5), 3327-3329. DOI: 10.1109/20.42292

Lai, W. Z., Wang, P., Zhao, W., Leng, Y. H., Huang, J., and Li, G. X. (2009). "Thermolysis synthesis of shape-controlled Fe-Ni alloy nanoparticles and magnetic property," *Chinese Journal of Inorganic Chemistry* 25(10), 1703-1710. DOI: 10.3321/j.issn:1001-4861.2009.10.001 (in Chinese)

Liao, Q., Tannenbaum, R., and Wang, Z. L. (2006). "Synthesis of $FeNi_3$ alloyed nanoparticles by hydrothermal reduction," *J. Phys. Chem. B* 110(29), 14262-14265. DOI: 10.1021/jp0625154

Liu, L., Guan, J., Shi, W., Sun, Z., and Zhao, J. (2010). "Facile synthesis and growth mechanism of flowerlike Ni-Fe alloy nanostructures," *J. Phys. Chem. C* 114(32), 13565-13570. DOI: 10.1021/jp104212v

Mamin, H. J., Rugar, D., Stern, J. E., Fontana, R. E., and Kasiraj, P. (1989). "Magnetic force microscopy of thin permalloy films," *Applied Physics Letters* 55(3), 318-320. DOI:10.1063/1.101898

Mohammadi, M., Ghasemi, A., and Tavoosi, M. (2016). "Mechanochemical synthesis of nanocrystalline Fe and F-B magnetic alloys," *J. Magn. Magn. Mater* 419, 189-197. DOI:10.1016/j.jmmm.2016.06.037

Moustafa, S. F., and Daoush, W. M. (2007). "Synthesis of nano-sized Fe-Ni powder by chemical process for magnetic applications," *Journal of Materials Processing Technology* 181(1-3), 59-63.DOI:10.1016/j.jmatprotec.2006.03.008

Nagasawa, C., Kumagai, Y., Urabe, K., and Shinagawa, S. (1999). "Electromagnetic shielding particleboard with nickel-plated wood particles," *Journal of Porous Materials* 6(3), 247-254.DOI:10.1023/A:1009692232398

Pan, Y. F, Wang, X., and Huang, J. T. (2016). "The preparation, characterization, and influence of multiple electroless nickel-phosphorus (Ni-P) composite coatings on poplar veneer," *BioResources* 11(1), 724-735. DOI: 10.15376/biores.11.1.724-735

Qin, G. W., Pei, W. L., Ren, Y. P., Shimada, Y., Endo, Y., Yamaguchi, M., Okamoto, S., and Kitakamic, O. (2009). "Ni80Fe20 permalloy nanoparticles: Wet chemical preparation, size control and their dynamic permeability characteristics when composited with Fe micron particles," *J. Magn. Magn. Mater* 321(24), 4057-4062. DOI:10.1016/j.jmmm.2009.08.004

Shi, C., Wang, L., and Wang, L. (2015). "Preparation of corrosion-resistant, EMI shielding and magnetic veneer-based composite via Ni–Fe–P alloy deposition," *J. Mater. Sci.: Mater. Electron* 26(9), 7096-7103. DOI: 10.1007/s10854-015-3331-6

Vitta, S., Khuntia, A., Ravikumar, G., and Bahadur, D. (2008). "Electrical and magnetic properties of nanocrystalline $Fe_{100-x}Ni_x$ alloys," *J. Magn. Magn. Mater*, 320(3-4), 182-189. DOI: 10.1016/j.jmmm.2007.05.021

Wang, H., Li, J., Kou, X., and Zhang, L. (2008). "Synthesis and characterizations of size-controlled $FeNi_3$ nanoplatelets," *J. Cryst. Growth* 310(12), 3072-3076. DOI: 10.1016/j.jcrysgro.2008.03.015

Wang, L., Jian, L., and Liu, H. (2011). "A simple process for electroless plating nickel-phosphorus film on wood veneer," *Wood Science & Technology* 45(1) 161-167. DOI: 10.1007/s00226-010-0303-0

Wang, L., and Li, J. (2013). "Electromagnetic-shielding wood-based material created using a novel electroless copper plating process," *BioResources* 8(3), 3414-3425. DOI: 10.15376/biores.8.3.3414-3425

Wang, L., Shi, C., and Wang, L. (2015). "Fabrication of magnetic and EMI shielding wood-based composite by electroless Ni–Fe–P plating process," *BioResources* 10(1), 1869-1878. DOI: 10.15376/biores.10.1.1869-1878

Wei, X. W., Zhu, G. X., Zhou, J. H., and Sun, H. Q. (2006). "Solution phase reduction to Fe-Ni alloy nanostructures with tunable shape and size," *Mater. Chem. Phys* 100(2-3), 481-485. DOI: 10.1016/j.matchemphys.2006.01.030

Xue, L., Yang, W., Liu, H., Men, H., Wang, A., Chang, C., and Shen, B.A. (2016). "Effect of Co addition on the magnetic properties and microstructure of FeNbBCu nanocrystalline alloys," *J. Magn. Magn. Mater* 419, 198-201. DOI: 10.1016/j.jmmm.2016.06.020

Zhou, P. H., Deng, L. J., Xie, J. L., Liang, D. F., Chen, L., and Zhao, X. Q. (2005). "Nanocrystalline structure and particle size effect on microwave permeability of FeNi powders prepared by mechanical alloying," *J. Magn. Magn. Mater* 292, 325-331. DOI: 10.1016/j.jmmm.2004.11.148

Zhou, S., Zhang, Q., Feng, L., and Huang, J. (2009). "Structure and magnetic property of FeNi nanoparticles," *Journal of Wuhan University* 55(3), 258-262. DOI: 10.3321/j.issn:1671-8836.2009.03.002 (in Chinese)

Article submitted: December 5, 2016; Peer review completed: January 21, 2017; Revised version received and accepted: February 10, 2017; Published: March 13, 2017.
DOI: 10.15376/biores.12.2.3154-3165